Text S1. Details of the numerical model

The model is a depth resolved version of the microbial minimum model (MinMod) developed by T.F. Thingstad and colleagues (Thingstad & Rassoulzadegan 1999, Thingstad et al. 2007, Thingstad et al. 2020) that has been extended with state variables for fish and detritus (see Fig. 1 in main text). The state variables of the model are listed in Table S1. The equations of the biological source and sink terms, Eq. S1 - S34, are listed in Table S2, S3 and S4. Values of the model coefficients and the forcing variables are given in Table S5 and S6.

Except for fish (see below), the change in a state variable (X_i) as a function of time (t) and depth (z) is represented by the partial differential equation:

$$\frac{\partial X_i}{\partial t} = B(X_i) + \frac{\partial}{\partial z}\kappa\frac{\partial X_i}{\partial z} - v_{X_i}\frac{\partial X_i}{\partial z} \qquad \text{(S34)}$$

Here, $B(X_i)$ is the biological source and sink terms (Table S2), κ is the turbulent diffusivity coefficient, and v_{X_i} is gravitational sinking rate, which is non-zero only for slow- and fast-sinking detritus.

Depth resolution necessitates two extensions of the original MinMod, i) representation of gravitational sinking of detritus and ii) representation of light, light limited growth, and self-shading of the photoautotrophs. To represent the migrant flux of carbon, we make use of an implicit representation of DVM that is based on acoustical observations.

Gravitational sinking of detritus and categorization of metabolic losses

Food ingested by the phagotrophs (heterotrophic flagellates, ciliates, copepods, and fish) is allocated to growth according to a yield-coefficient (Y_i) that is specific for each organism group. In the original MinMod, the fractions of the food ingested (I_i) not allocated to growth, $(1\text{-}Y_i)I_i$, are instantaneously remineralized as DIP (state variable with symbol *P,* Table S1). In our depth resolved version, dissolved losses enter DIP as in the original MinMod, while particulate losses enter detritus (Fig. S2, Table S4) that is affected by gravitational sinking. We assume that the carbon loss follows the phosphorus loss according to Redfield ratio. Carbon not lost to detritus, is lost as l-DOC and CO_2 (by respiration), of which the latter is not an explicit state variable in the model but depletes dissolved oxygen according to a respiratory coefficient (RQ). The sum of the losses of l-DOC and CO_2 corresponds, in Redfield proportion, to the organism excretion of phosphorus to DIP. Bacteria consumes l-DOC (Fig S2), and their respiratory CO_2 loss is calculated according to a yield (Y_{BC}) reflecting the bacterial growth efficiency (BGE) as well as their carbon to phosphorus ratio (Eq. S29 of Table S4).

Light limited growth and phytoplankton self-shading

Light-limited phytoplankton growth is not part of the original MinMod and is here introduced together with nutrient limitation in accordance with the minimum principle, i.e., the most limiting factor becomes determine growth rate (Eq. S17 and S18 of Table S3). The light intensity E as a function of depth (z) is calculated according to

$$E(z) = E_0 \, exp\left(-\int_0^z K(\sigma)d\sigma\right) \quad \text{(S35)}$$

where E_0 is the light intensity just below the surface and σ is an integration variable accounting for the non-uniform distribution of the light attenuation (K) with depth. The depth specific light attenuation was calculated with the empirical expression of (Morel & Maritorena 2001):

$$K = K_w + k_p Chl^{k_e} \quad \text{(S36)}$$

where K_w is attenuation of pure water, Chl (mg m^{-3}) is depth specific chlorophyll concentration (mg m^{-3}), and k_p and k_e are wavelength-specific constants (Table S5). We applied the coefficients for 440 nm in (Morel & Maritorena 2001), which is approximately the midpoint of the waveband peak that most classes of algae have in their photosynthetic action spectrum (Kirk, 2011). This 440 nm parameterisation provided good correspondence with the observed PAR light penetration in the Red Sea (Fig. S3). In the model, chlorophyll concentration was obtained by converting the simulated biomass of the autotrophic non-diatoms (A) and the diatoms (D) into Chl, i.e., where $Chl = \rho_{ChlP}\,(A+D)$ and ρ_{ChlP} (mg-Chl/µmol-P) is a conversion factor (Table S5).

Implicit representation of fish-DVM based on acoustical observations.

The model simulates active carbon flux according to the DVM carried out by the mesozooplanktivorous organism group representing mesopelagic fish in the depth resolved model. While fish abundance is a dynamic state variable determined by food intake and mortality (Eq. S7), their vertical distribution is constrained by acoustical observations with an implicit representation of DVM. From the DVM pattern given by the acoustical observations (Fig. S4A), we calculated the average relative depth distribution over a 24h cycle (Fig. S4B). This frequency distribution, $f(z)$, where z is depth and $\int f(z)dz = 1$, represents the fraction of time spent at the different depths during the 24 hours cycle, i.e., a "time allocation vector". The simulated fish abundance (µmol P m^{-3}) at depth z is then $F(z) = F_{int}\, f(z)$, where F_{int} is the total simulated fish biomass over the entire water column (µmol P m^{-2}). Total fish ingestion (µmol P m^{-2} h^{-1}) of the

water column is $I_{F\_int} = \int I_F(z)F(z)dz$ where $I_F(z)$ is the ingestion rate that is calculated from the depth specific encounter rate with their prey (mesozooplankton). The growth (µmol P m^{-2} h^{-1}) of the entire fish stock (before mortality) is $Y_F I_{Fint}$, where Y_F is the yield allocated for growth. For each time step in the numerical realization, this total growth is distributed over the water column according to the time allocation vector, $f(z)$, so that the change in fish concentration at depth z is:

$$\frac{\partial F(z)}{\partial t} = Y_F I_{Fint} f(z) - \delta_F F(z) \quad \text{(S37)}$$

where δ is the fish mortality rate.

The ingested food not allocated to growth, is lost also according to the time allocation vector, $f(z)$. This loss, $(1 - Y_F)I_{Fint}f(z)$, is further categorized as defecation, excretion, and respiration as for the other phagotrophs of the model (Table S4).

Calculation of simulated active carbon flux

The active flux at a certain depth, $z = x$, is calculated from the discrepancy between the depth distributions of feeding and metabolic losses of the fishes below depth x. The more of the feeding takes place above depth x, the larger the active carbon flux at this depth. If simulated zooplankton mainly distributes in the epipelagic zone, most fish feeding will take place there, and the larger the active flux out of the epipelagic zone will be. The simulated fish losses, however, distribute vertically according to the time spent at depth as given by the acoustical observations. Since fish feeding is also allowed to take place in the mesopelagic zone (to the extent simulated mesozooplankton are present), part of what is lost in the mesopelagic originates from food ingested in the mesopelagic and is not counted as active flux. Accordingly, we define the depth specific active flux (µmol P m^{-2} h^{-1}) at a depth x as the sum of all fish losses (respiration, excretion, defecation, and mortality) that takes place below this depth minus the food intake that takes place below the same depth:

$$Active\_flux_{z=x} = \int_{z=x}^{\infty} (1 - Y_F)I_{F_{int}} f(z)d + \int_{z=x}^{\infty} \delta F(z)dz - \int_{z=x}^{\infty} I_F(z)F(z)dz \quad \text{(S38)}$$

The first integral represents respiration, excretion, and defecation, the second and third integral represent mortality loss and food consumed below depth x respectively.

Model output related to carbon export

For the simulated scenarios, we report a set of metrics related to carbon export and sequestration in Table 1 and 2 of the main text:
Net primary production (NPP) is the net growth of autotrophs, represented by non-diatoms and diatoms in the model.
Euphotic depth is the depth where 0.1% of the surface light penetrates (Buesseler et al. 2020).
Total carbon export is the total net downward carbon flux as a function of depth. It is calculated as the sum of the gravitational flux of slow- and fast-sinking detritus, the net downward diffusive flux of suspended detritus, the net downward diffusive flux of DOC, and the net downward active flux.
Active flux through a particular depth is defined as the sum of all fish losses (respiration, excretion, defecation, and mortality) minus the food intake taking place deeper than this depth.
Total phosphorus export is the net downward phosphorus flux of DIP and the phosphorus content of detritus and organisms.
Net upward DIP flux is the net upward diffusive transport of DIP at a certain depth which in steady state equals the total phosphorus export at the same depth. It serves as a proxy for new production (Dugdale & Goering 1967, Eppley & Peterson 1979).
Gravitational flux attenuation is the exponent of the exponential expression fitted to the simulated gravitational flux and is reported for the depth interval between 200 and 700 m depth in Table 1 and 2 of the main text.
Gravitational flux penetration length scale is the reciprocal of the gravitational flux attenuation.
Community respiration below 200 m depth is the depth integrated respiration of all organisms below 200 m depth. This quantity also includes the carbon export at 700 m depth.
WMDR is the weighted mean depth of the community respiration below 200 m depth
A sequestration proxy approximates the carbon sequestered by the BCP. By using the open-ocean relationship between depth and sequestration time (fig. 2b in (Boyd et al. 2019), we approximated the corresponding sequestration time (in years) for the WMRD. The reported sequestration proxy (with unit kg C m^{-2}) is the product of this sequestration time and the integrated mesopelagic community respiration. As described in Methods, this estimate corresponds to the simulated water column being placed in the open ocean rather than in the enclosed Red Sea. The water renewal mechanisms and ventilation of the Red Sea water masses are different from that of the open ocean. The sequestration proxy is therefore not suitable for assessing actual carbon sequestration in the Red Sea but is used to compare simulated scenarios.

Literature cited

Boyd PW, Claustre H, Levy M, Siegel DA, Weber T (2019) Multi-faceted particle pumps drive carbon sequestration in the ocean. Nature 568:327-335

Buesseler KO, Boyd PW, Black EE, Siegel DA (2020) Metrics that matter for assessing the ocean biological carbon pump. Proceedings of the National Academy of Sciences 117:9679-9687

Calleja ML, Al-Otaibi N, Morán XAG (2019) Dissolved organic carbon contribution to oxygen respiration in the central Red Sea. Scientific reports 9, Article number: 4690

Dugdale RC, Goering JJ (1967) Uptake of new and regenerated forms of nitrogen in primary productivity. Limnology and Oceanography 12:196-206

Dypvik E, Kaartvedt S (2013) Vertical migration and diel feeding periodicity of the skinnycheek lanternfish (Benthosema pterotum) in the Red Sea. Deep-Sea Research Part I-Oceanographic Research Papers 72:9-16

Eppley RW, Peterson BJ (1979) Particulate organic matter flux and planktonic new production in the deep ocean. Nature 282:677-680

Klevjer TA, Torres DJ, Kaartvedt S (2012) Distribution and diel vertical movements of mesopelagic scattering layers in the Red Sea. Marine Biology 159:1833-1841

Morel A (1988) Optical Modeling of the Upper Ocean in Relation to Its Biogenous Matter Content (Case-I Waters). Journal of Geophysical Research-Oceans 93:10749-10768

Morel A, Maritorena S (2001) Bio-optical properties of oceanic waters: A reappraisal. Journal of Geophysical Research: Oceans 106:7163-7180

Thingstad TF, Havskum H, Zweifel UL, Berdalet E, Sala MM, Peters F, Alcaraz M, Scharek R, Perez M, Jacquet S, Flaten GAF, Dolan JR, Marrasé C, Rassoulzadegan F, Hagstrøm Å, Vaulot D (2007) Ability of a "minimum" microbial food web model to reproduce response patterns observed in mesocosms manipulated with N and P, glucose, and Si. Journal of Marine Systems 64:15-34

Thingstad TF, Rassoulzadegan F (1999) Conceptual models for the biogeochemical role of the photic zone microbial food web, with particular reference to the Mediterranean Sea. Progress in Oceanography 44:271-286

Thingstad TF, Vage S, Bratbak G, Egge J, Larsen A, Nejstgaard JC, Sandaa RA (2020) Reproducing the virus-to-copepod link in Arctic mesocosms using host fitness optimization. Limnology and Oceanography 66: S303-S313.

Table S1. State variables (with accompanying symbols) of the depth resolved MinMod. "M" marks variables of the original MinMod described in Thingstad et al (2007, 2020).

Symbol		Meaning	Unit
P	M	Dissolved inorganic phosphate (DIP)	µmol-P m^{-3}
B	M	Heterotrophic bacteria	µmol-P m^{-3}
A	M	Autotrophic non-diatoms	µmol-P m^{-3}
D	M	Diatoms	µmol-P m^{-3}
H	M	Heterotrophic flagellates	µmol-P m^{-3}
C	M	Ciliates	µmol-P m^{-3}
Z	M	Mesozooplankton	µmol-P m^{-3}
F		Fish (i.e., all mesozooplanktivorous organisms)	µmol-P m^{-3}
Det_s		Slow sinking detritus	µmol-P m^{-3}
Det_f		Fast sinking detritus	µmol-P m^{-3}
Det_n		Suspended detritus (non-sinking)	µmol-P m^{-3}
L	M	Labile dissolved organic carbon (l-DOC)	µmol-C m^{-3}
S	M	Silicate	µmol-Si m^{-3}
E		Irradiance	µmol quanta m^{-2} s^{-1}
O		Dissolved O_2	µmol-O_2 m^{-3}
S_{opal}		Biogenic Si-content of fast sinking detritus	µmol-Si m^{-3}

Table S2. The differential equations of the state variables. Here, these are expressed as ordinary differential equations as a function of time. The right side represents the biological source and sink terms which correspond to $B(X_i)$ in the partial differential equation also accounting for depth (Eq. 1 in the main text).

$$\frac{dB}{dt} = \mu_B B - I_H H \quad \text{(S1)}$$

$$\frac{dA}{dt} = \mu_A A - \frac{A}{A+H} I_C C \quad \text{(S2)}$$

$$\frac{dD}{dt} = \mu_D D - \frac{D}{D+\sigma C} I_Z Z - \delta_D D \quad \text{(S3)}$$

$$\frac{dH}{dt} = Y_H I_H H - \frac{H}{A+H} I_C C \quad \text{(S4)}$$

$$\frac{dC}{dt} = Y_C\, I_C C - \frac{\sigma C}{D+\sigma C} I_Z Z \quad \text{(S5)}$$

$$\frac{dZ}{dt} = Y_Z I_Z Z - I_F F \quad \text{(S6)}$$

$$\frac{dF}{dt} = Y_F I_F F - \delta_F F \quad \text{(S7)}$$

$$\frac{dDet_s}{dt} = P_{HC} + k_{frag}\left(Det_f - Det_s\right) \quad \text{(S8)}$$

$$\frac{dDet_f}{dt} = \delta_D D + P_Z + P_F + \delta_F F - k_{frag} Det_f \quad \text{(S9)}$$

$$\frac{dDet_n}{dt} = k_{frag} Det_s - k_l Det_n \quad \text{(S10)}$$

$$\frac{dP}{dt} = -\left(\frac{dB}{dt} + \frac{dA}{dt} + \frac{dD}{dt} + \frac{dH}{dt} + \frac{dC}{dt} + \frac{dZ}{dt} + \frac{dF}{dt} + \frac{dDet_s}{dt} + \frac{dDet_f}{dt} + \frac{dDet_n}{dt}\right) \quad \text{(S11)}$$

$$\frac{dL}{dt} = f_{coc}\rho_{CP}(\mu_A A + \mu_D D) + k_l \rho_{CP} Det_n + Doc_{HCZ} + Doc_F - \frac{1}{Y_{BC}}\mu_B B \quad \text{(S12)}$$

$$\frac{dS}{dt} = k_{opal} S_{opal} - \rho_{DS}\mu_D D \quad \text{(S13)}$$

$$\frac{dS_{opal}}{dt} = \rho_{DS}\delta_D D + \rho_{DS}\frac{D}{D+\sigma C} I_Z Z - k_{opal} S_{opal} \quad \text{(S14)}$$

$$\frac{dO}{dt} = P_Q \rho_{CP}(\mu_A A + \mu_D^E D) - \frac{1}{R_Q}(R_B + R_{HCZ} + R_F) \quad \text{(S15)}$$

Table S3. Specific growth and ingestion rates.

$$\mu_B = \mu_B^m \cdot min\left(\frac{P}{\frac{\mu_B^m}{\alpha_P} + P}, \frac{L}{\frac{\mu_B^m}{\alpha_{BL}} + L}\right) \quad \text{(S16)}$$

$$\mu_A = \mu_A^m \cdot min\left(\frac{P}{\frac{\mu_A^m}{\alpha_{AP}} + P}, \frac{E}{\frac{\mu_A^m}{\alpha_{AE}} + E}\right) \quad \text{(S17)}$$

$$\mu_D = \mu_D^m \cdot min\left(\frac{P}{\frac{\mu_D^m}{\alpha_{DP}} + P}, \frac{S}{\frac{\mu_D^m}{\alpha_{Ds}} + S}, \frac{E}{\frac{\mu_D^m}{\alpha_{DE}} + E}\right) \quad \text{(S18)}$$

$$I_H = I_H^m \cdot \frac{B}{\frac{I_H^m}{\alpha_H} + B}, \qquad I_H^m = \mu_H^m / Y_H \quad \text{(S19)}$$

$$I_C = I_C^m \cdot \frac{A + H}{\frac{I_C^m}{\alpha_C} + A + H}, \qquad I_C^m = \mu_C^m / Y_C \quad \text{(S20)}$$

$$I_Z = I_Z^m \cdot \frac{\sigma C + D}{\frac{I_Z^m}{\alpha_Z} + \sigma C + D}, \qquad I_Z^m = \mu_Z^m / Y_Z \quad \text{(S21)}$$

$$I_F = I_F^m \cdot \frac{Z}{\frac{I_F^m}{\alpha_F} + Z}, \qquad I_F^m = \mu_F^m / Y_F \quad \text{(S22)}$$

Table S4. Allocation of metabolic losses. Total loss is ingested material not incorporated as biomass of the organism, i.e., fecal, excreted, and respired material. Organism excretion of phosphorus back into DIP is taken care of by the mass balance expressed in Eq. S11 and corresponds, by Redfield ratio, to the combined carbon loss by respiration and DOC excretion.

Total losses (µmol-P m^{-3} h^{-1})		
from *H* and *C*:	$T_{HC} = (1 - Y_H)I_H H + (1 - Y_C)I_C C$	(S23)
from *Z*:	$T_Z = (1 - Y_Z)I_Z Z$	(S24)
from *F*:	$T_F = (1 - Y_F)I_F F$	(S25)
Particulate losses to detritus (µmol-P m^{-3} h^{-1})		
from *H* and *C* to Det_s:	$P_{HC} = f_d T_{HC}$	(S26)
from *Z* to Det_f:	$P_Z = f_d T_Z$	(S27)
from *F* to Det_f:	$P_F = f_d T_F$	(S28)
Respiration losses (µmol-C m^{-3} h^{-1})		
from B:	$R_B = \left(\frac{1}{Y_{BC}} - \rho_B\right)\mu_B B$	(S29)
from *H*, *C* and *Z*:	$R_{HCZ} = \rho_{CP} f_{rHCZ}(T_{HC} + T_Z)$	(S30)
from *F*:	$R_F = \rho_{CP} f_{rF} T_F$	(S31)
DOC losses to *L* (µmol-C m^{-3} h^{-1})		
from *H*, *C* and *Z*:	$Doc_{HCZ} = \rho_{CP}(1 - f_d - f_{rHCZ})(T_{HC} + T_Z)$	(S32)
from *F*:	$Doc_F = \rho_{CP}(1 - f_d - f_{rF})T_F$	(S33)

Table S5. Coefficients and their values of the depth resolved MinMod ("M" mark coefficients common to the original MinMod described in Thingstad et al (2007, 2020). Letters used in 'Meaning' column correspond to variables defined in Table S1.

Symbol		Meaning	Value	Unit	Values in Thingstad et al 2007	2020
		Affinity/clearance rates for osmotrophs/phagotrophs (at 17ºC for those marked M*)*				
α_{BP}	M	Bacterial affinity for *P*	0.08	m^3 µmol-P h^{-1}	0.08	0.08
α_{BL}	M	Bacterial affinity for *L*	$1.6\ 10^{-6}$	m^3 µmol-P h^{-1}	$5.3\ 10^{-6}$	$8\ 10^{-5}$
α_{AP}	M	Autotrophic non-diatom affinity for *P*	0.04	m^3 µmol-P h^{-1}	0.04	0.04
α_{AE}		Autotrophic non-diatom affinity for *E*	0.0051	h^{-1}/(µmol quanta $m^{-2}s^{-1}$)		
α_{DP}	M	Diatom affinity for *P*	0.03	m^3 µmol-P h^{-1}	0.03	0.03
α_{DS}	M	Diatom affinity for *S*	0.0019	m^3 µmol-P h^{-1}	0.0012	0.0019
α_{DE}		Diatom affinity for *E*	0.0057	h^{-1}/(µmol quanta $m^{-2}s^{-1}$)		
α_{HB}	M	Heterotrophic flagellate clearance rate for *B*	0.0015	m^3 µmol-P^{-1} h^{-1}	0.0015	0.0015
α_C	M	Ciliate clearance rate for *A* and *H*	0.00045	m^3 µmol-P^{-1} h^{-1}	0.0005	0.00045
α_Z	M	Mesozooplankton clearance rate for *D*	0.00015	m^3 µmol-P^{-1} h^{-1}	0.00015	0.00015
σ	M	Mesozoopl. selectivity factor for *C* relative to *D*	2	Dimensionless	2	2
α_F		Fish clearance rate for *Z*	0.00037	m^3 µmol-P^{-1} h^{-1}		
		Maximum growth/ingestion rates (at 17ºC)				
μ_B^m	M	Maximum growth rate bacteria	0.25	h^{-1}	0.25	0.25
μ_A^m	M	Maximum growth rate autotrophic non-diatoms	0.054	h^{-1}	0.054	0.054
μ_D^m	M	Maximum growth rate diatoms	0.06	h^{-1}	0.06	0.06
μ_H^m	M	Maximum growth rate heterotrophic flagellates	0.132	h^{-1}	0.132	0.132
μ_C^m	M	Maximum growth rate ciliates	0.045	h^{-1}	0.045	0.045
μ_Z^m	M	Maximum growth rate mesozooplankton	0.00625	h^{-1}	0.00625	0.0625
μ_F^m		Maximum growth rate fish	0.00225	h^{-1}		
		Yields (fraction of ingested that is allocated to growth)				
Y_H	M	Heterotrophic flagellates	0.4	Dimensionless	0.3	0.4
Y_C	M	Ciliates	0.3	Dimensionless	0.2	0.3
Y_Z	M	Mesozooplankton	0.15	Dimensionless	0.15	0.15
Y_F		Fish	0.15	Dimensionless		
Y_{BC}	M	Bacterial yield on *L* (*l-DOC*) (BGE = $\rho_B\ Y_{BC}$)	0.001	Dimensionless	0.004	
		Losses to detritus (POP, POC) respiration (CO2, DIP) and dissolved (l-DOC, DIP)				
f_{coc}		Photosynthetic carbon overflow	1	Dimensionless		
f_d		Fraction of total loss that enters detritus	0.2	Dimensionless		
f_{rHCZ}		Fraction of total loss that is respired (plankton)	0.6	Dimensionless		
f_{rF}		Fraction of total loss that is respired (fish)	0.4	Dimensionless		
		Detritus sinking and remineralisation				
δ_D		Diatom mortality (transfer to Det_f and S_{opal})	0.01/24	h^{-1}		
k_{opal}		Dissolution rate of S_{opal}	0.25/24	h^{-1}		

v_{Dets}		Sinking speed of slow sinking detritus	10/24	m h^{-1}		
v_{Detf}		Sinking speed of fast sinking detritus	100/24	m h^{-1}		
k_l		Leakage rate from suspended detritus to *P* and *L*	0.02/24	h^{-1}		
k_{frag}		Fragmentation rate of Det_s and Det_f	0.3/24	h^{-1}		
		Temperature effect				
$Q_{10\alpha}$	M	Q_{10} for affinities and clearance rates	1.4			1.4
$Q_{10\max}$	M	Q_{10} for maximum growth and ingestion rates	1.9			1.9
		Light attenuation coefficients (Morel & Maritorena 2001)				
K_w		Attenuation from pure water	0.00885	m^{-1}		
k_p, k_e		Empirical coefficients related to chlorophyll light absorption	0.11, 0.67			
		Oxygen production and consumption (affects no state-variables other than O_2)				
P_Q		Photosynthetic quotient	1.4	mol-O_2/mol-C		
R_Q		Respiratory quotient	0.876	mol-C/mol-O_2		
		Stoichiometric ratios and conversion factors				
ρ_B	M	Molar carbon:phosphorus ratio in *B*	50	mol-C/mol-P	50	
ρ_{CP}	M	Molar carbon:phosphorus ratio	106	mol-C/mol-P	106	106
ρ_{DS}	M	Molar silicate:phosphorus ratio in *D*	16	mol-P/mol-Si	16	25
ρ_{ChlP}	M	Ratio between Chl and phosphorus in *A* and *D*	1/63	mg-Chl /μmol-P	1/47	1/47

Table S6. Forcing variables and their values in the baseline scenario. In the no-fish scenario, the mesozooplankton mortality (being the top predator) was 0.03 d^{-1} corresponding to a turnover time for the mesozooplankton biomass of ~5 weeks.

Symbol	Meaning	Value	Unit	
	Forcing variables			
E_0	Irradiance just below surface	600	µmol quanta m^{-2} s^{-1}	
K_{other}	Attenuation other than from pure water and Chl	0	m^{-1}	
κ	Turbulent diffusivity	3×10^{-4}	m^2 s^{-1}	
T	Temperature	Observed depth profile (Fig.S1B)	°C	
P_b, S_b	Inorganic phosphate and silicate concentrations at deep boundary (700 m)	1.0 10.7	µmol-P m^{-3} µmol-Si m^{-3}	
δ_F	Mortality rate of mesopelagic fish	2	yr^{-1}	
$f(z)$	Vertical distribution of fish	Observed depth profile (Fig. S1J)	Dimensionless	

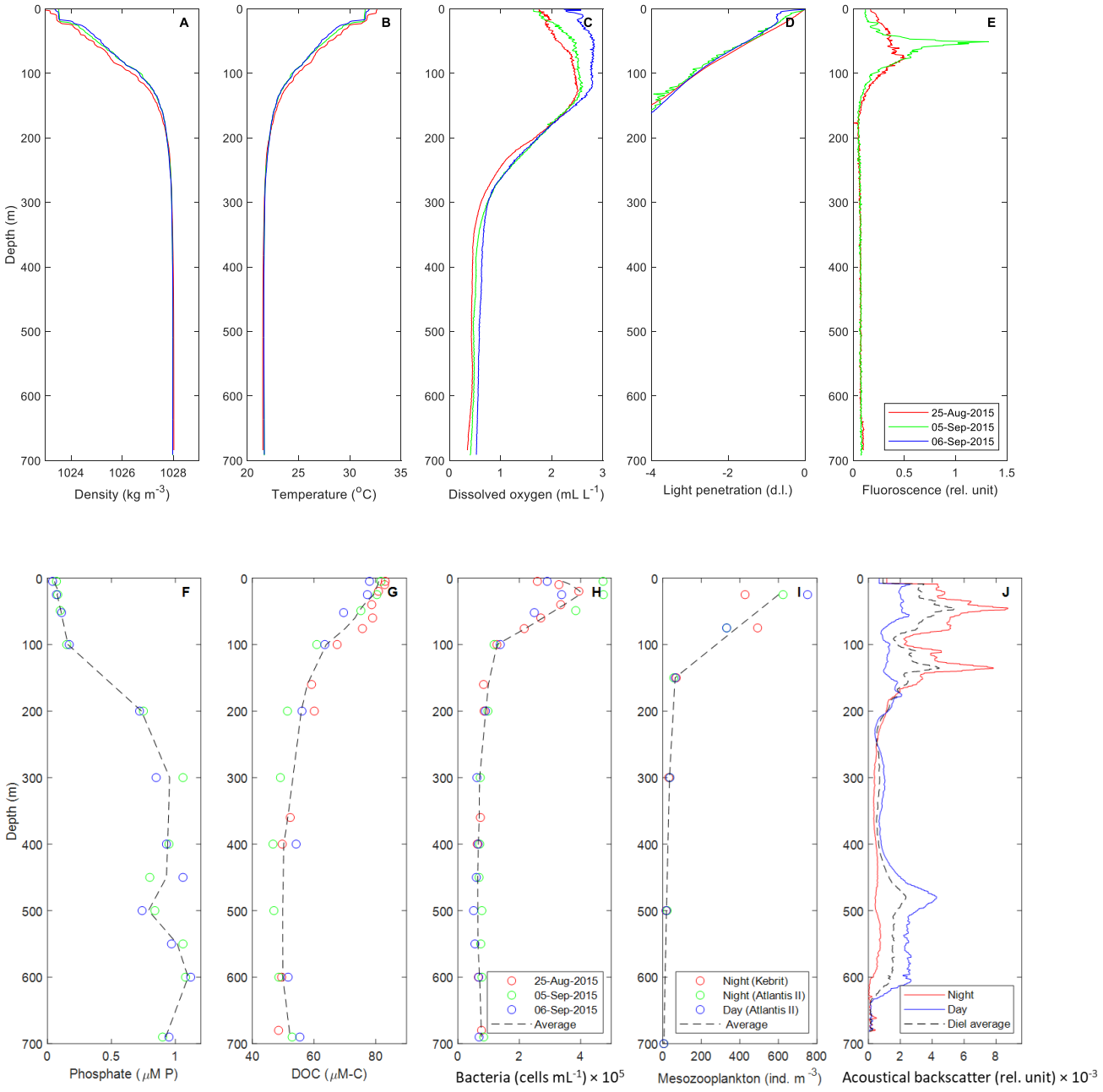

Fig. S1. Red Sea water column characteristics. Observations in August and September 2015 from (Calleja et al. 2019) (A-H) at station KAEC (22.47 °N 39.03 °E). Observations of dissolved oxygen, phosphate (DIP), DOC and heterotrophic bacteria are from Sept 5 and 6, 2015. Mesozooplankton observations (I) are from table 2 in (Dypvik & Kaartvedt 2013) collected at locations north (Kebrit, 24.48°N 36.15°E) and south (Atlantis, 21.27°N 38.5°E) of KAEC. Acoustical backscatter (J) was obtained at KAEC. Night, Day and Diel refer to the depth distributions averaged for the time periods 18-6h, 6-18h and 0-24h respectively and provide a relative measure of the time spent at different depths during the three periods (see Fig. S4). Light penetration (D) is dimensionless (d.l.) and expressed at a logarithmic scale according to $\log_{10}(E_z/E_0)$ where E_0 is the surface irradiance and E_Z is the irradiance at depth z.

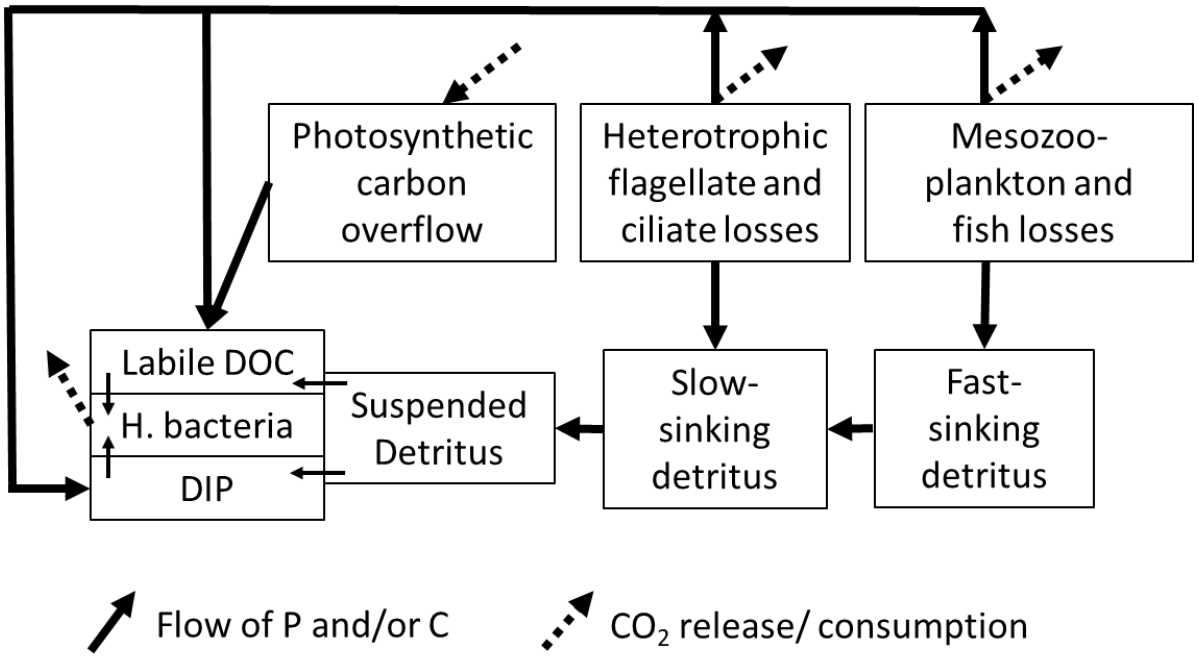

Fig. S2. Formation, fragmentation, and remineralisation of DOC and detritus. The total losses of heterotrophic flagellates, ciliates, mesozooplankton, and fish correspond to ingested food not allocated to growth. Organism phosphorus is lost to detritus and DIP, while organism carbon is lost to detritus, DOC, and CO_2. Sinking diatoms (parameterized as mortality, see text) fuel the fast-sinking detritus and opal but are not indicated in the illustration.

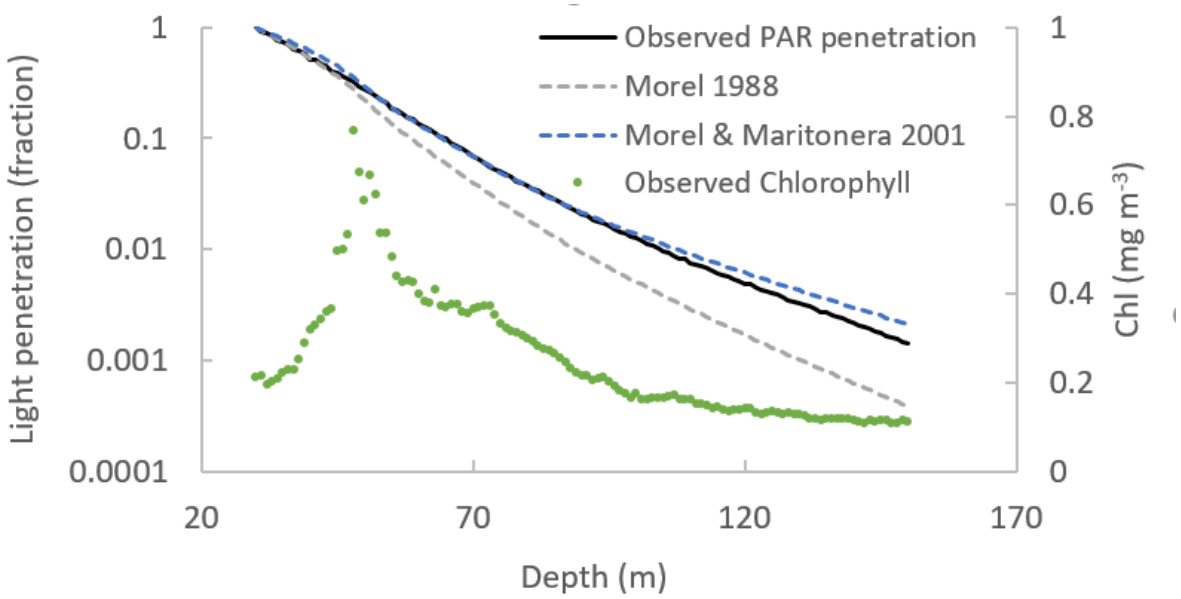

Fig. S3. Parameterization of self-shading by photoautotrophs. Observed PAR light penetration (solid line) and chlorophyll (green dots) at the Red Sea station KAEC (22.47 °N 39.03 °E, from Calleja et al. 2019). The blue broken line shows the predicted light penetration when we applied the relationship of Morel and Maritonera (2001) using the coefficients for 440 nm in Eq. S35 and S36. This relationship provided better relationship than that of (Morel 1988) (grey broken line) and was used to represent self-shading in our depth resolved model.

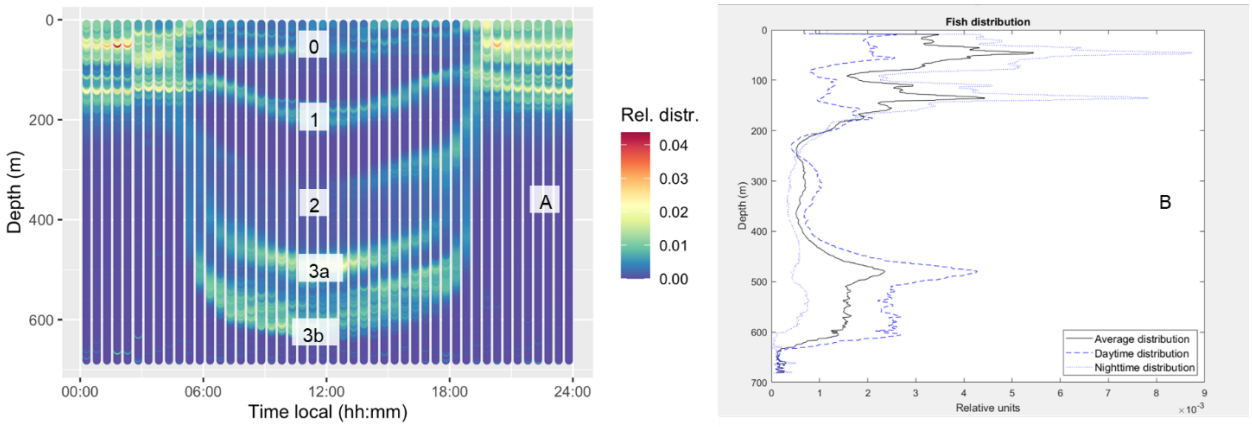

Fig. S4. Diel vertical migration (DVM) as indicated by acoustic backscatter. Distribution of acoustic backscatter during a diel cycle at the KAEC station (22.47 °N 39.03 °E) in the Red Sea (A) with associated day-, nighttime, and 24h average distributions (B). The 24h average distribution represents the fraction of time the organisms spend at the different depths of the water column and is referred to as the "time allocation vector" in the text. Previous studies (Klevjer et al. 2012, Dypvik & Kaartvedt 2013) suggest that the layers consist of species of the genera *Maurolicus* (layer 1), *Vinciguerra* (layer 2/3a) and *Benthosema* (layer 3a/3b). Layer 0 reflects non-migrating epipelagic organisms. The vertical lines group the backscatter into 48 temporal bins used to calculate time spent at the different depths (2 m resolution) during a diel cycle.

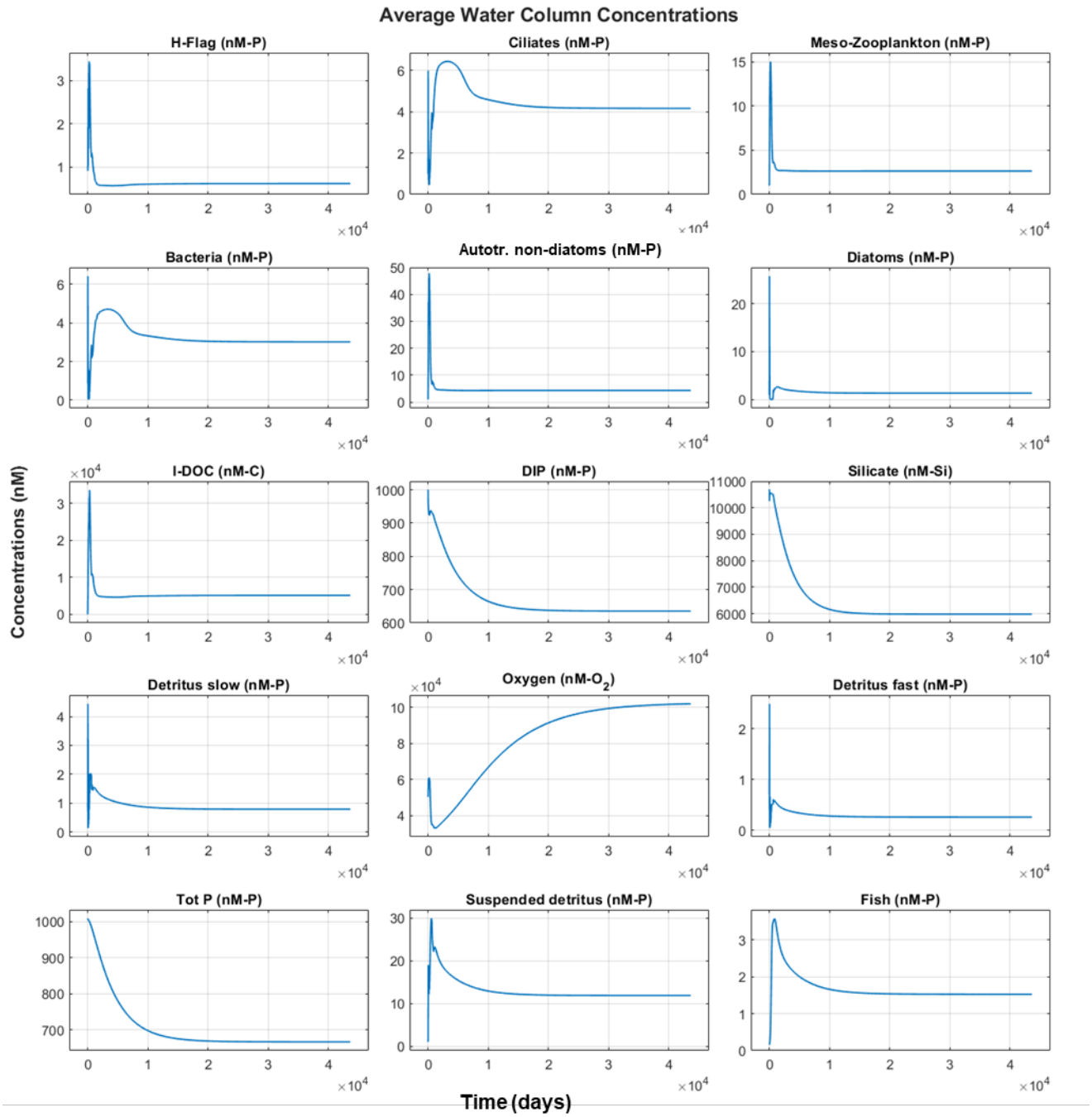

Fig. S5. Convergence towards the steady state solution for the baseline scenario. The vertical axis is the average concentrations of the water column (0 – 700 m). The x-axis is the number of simulated days after initialization of the model. The model was initialized with homogenous depth distributions for all state variables (except for fish, see main text). The steady state depth distributions are shown in Fig. S6.

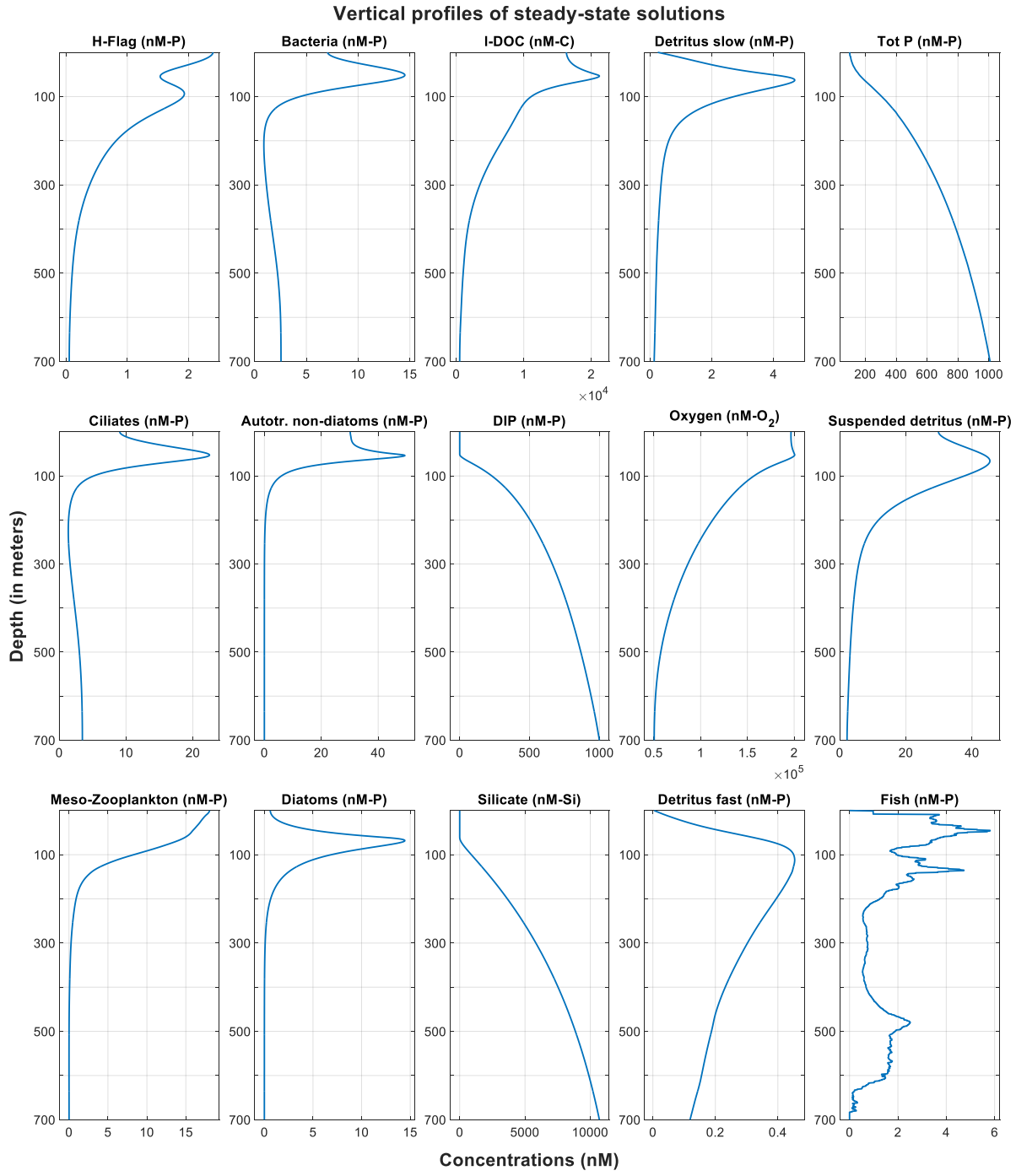

Fig. S6. Steady state depth distributions of the baseline simulation. The model was initialized with homogenous depth distributions for all state variables (except for fish, see main text). For comparison of the baseline scenario with observations see Fig. 2 in main text.